

This is the accepted manuscript made available via CHORUS. The article has been published as:

Disorder Quenching of the Charge Density Wave in $\text{ZrTe}_{\{3\}}$

Moritz Hoesch, Liam Gannon, Kenya Shimada, Benjamin J. Parrett, Matthew D. Watson,
Timur K. Kim, Xiangde Zhu, and Cedomir Petrovic

Phys. Rev. Lett. **122**, 017601 — Published 2 January 2019

DOI: [10.1103/PhysRevLett.122.017601](https://doi.org/10.1103/PhysRevLett.122.017601)

Disorder quenching of the Charge Density Wave in ZrTe_3

Moritz Hoesch,^{1,2,3} Liam Gannon,^{1,4} Kenya Shimada,² Benjamin Parrett,^{1,5}
Matthew D. Watson,^{1,6} Timur K. Kim,¹ Xiangde Zhu,^{7,*} and Cedomir Petrovic⁷

¹*Diamond Light Source, Harwell Campus,
Didcot OX11 0DE, United Kingdom*

²*Hiroshima Synchrotron Radiation Center,
Hiroshima University, 2-313 Kagamiyama,
Higashi-Hiroshima 739-0046, Japan*

³*DESY Photon Science, Deutsches Elektronen-Synchrotron,
Notkestrasse 85, 22607 Hamburg, Germany, moritz.hoesch@desy.de*

⁴*Clarendon Laboratory, University of Oxford Physics Department,
Parks Road, Oxford, OX1 3PU, United Kingdom*

⁵*London Centre for Nanotechnology and Department of Physics and Astronomy,
University College London, Gower Street, London WC1 E6BT, UK*

⁶*SUPA, School of Physics and Astronomy,
University of St. Andrews, St. Andrews KY16 9SS, United Kingdom*

⁷*Condensed Matter Physics and Materials Science Department,
Brookhaven National Laboratory Upton, NY 11973, USA*

(Dated: October 22, 2018)

Abstract

The charge density wave (CDW) in ZrTe_3 is quenched in samples with small amount of Te isoelectronically substituted by Se. Using angle-resolved photoemission spectroscopy we observe subtle changes in the electronic band dispersions and Fermi surfaces on Se substitution. The scattering rates are substantially increased, in particular for the large three-dimensional Fermi surface sheet. The quasi-one-dimensional band is unaffected by the substitution and still shows a gap at low temperature, which starts to open from room temperature. Long-range order is, however, absent in the electronic states as in the periodic lattice distortion. The competition between superconductivity and CDW is thus linked to the suppression of long-range order of the CDW.

The charge density wave (CDW) is a much studied self-organisation of metallic electrons in a crystalline solid [1, 2]. Besides electronic signatures it manifests itself as periodic lattice distortion (PLD) with a periodicity given by the CDW modulation. In the last decade the competition between CDWs and superconductivity (SC) has gained renewed attention, following observations of incommensurate PLDs in the copper oxide family of superconductors [3–5]. In a very simple picture a competition between CDW and SC may arise due to the removal of spectral weight from the Density of States at the Fermi level (DOS at E_F) if an energy gap is formed. Quenching the CDW restores DOS at E_F , which is required for SC. If it arises from static disorder this will also affect the SC properties, but these have been shown theoretically to be more robust, especially when considering electron correlations [6, 7]. In the extreme case of Josephson-linked networks of 1-dimensional chain segments, superconductivity is even found to be enhanced by disorder [8].

Besides the complex oxides cited above, competition between CDW and SC exists in simpler binary materials. Quenching of a CDW under pressure and concomitant emergence of SC has been found widely in transition-metal trichalcogenides [9, 10], rare-earth trichalcogenides [11–13] and layered transition-metal dichalcogenides [14]. The specific arrangement of electronic bands that form the CDW as well as the PLD vary widely between these materials thus establishing the competition as a fundamental principle of solid state physics.

The uniaxial material ZrTe_3 shows (filamentary) SC below about $T_c \simeq 2$ K at ambient pressure [17, 18]. The CDW is detected as an anomaly in resistivity around $T_{CDW} = 63$ K [17] with an incommensurate PLD modulation $\vec{q}_{CDW} \simeq (0.07, 0, 0.333)$ [19]. The resistivity continues to drop in a metallic fashion below T_{CDW} . The two main FS sheets are a hole-like sheet in the (a, b) -plane (3D) and a pair of electron-like and very flat sheets from quasi-one dimensional (q1D) bands [20–22]. Bulk SC emerges in ZrTe_3 when the CDW is quenched, *e.g.* at hydrostatic pressures above $P_c = 5$ GPa [10] or in disordered samples grown at high temperatures [23]. For the quenching of the CDW under pressure two potential mechanisms have been discussed: disorder [24, 25], or a re-arrangement of band fillings in the multi-sheet Fermi surface (FS) leading to the loss of the CDW stability [26]. In either scenario it is reasonable to assume that the SC involves electrons in the quasi-one-dimensional (q1D) sheets of the FS that have been identified as driving the CDW [20–22] and which show strong electron-phonon coupling (EPC) to low-energy vibrational modes [27, 28]. This electron-

lattice interaction probably contributes to stabilising the long wavelength (small q) CDW.

In this letter we access the regime of low disorder by light chemical substitution of Te with Se, $\text{ZrTe}_{3-x}\text{Se}_x$. A suppression of the CDW both in transition temperature and magnitude of the resistivity anomaly was reported [29]. Above $x = 0.02$ the CDW anomaly is removed and bulk multi-band BCS type SC with T_c up to 4.5 K emerges; the coupling is dominantly intraband with some interband contributions [29]. With the isoelectronic substitution only a slight rearrangement of carriers between FS sheets is expected. Below, we clarify these subtle changes, including a shift of the van-Hove-singularity (vHS) in the q1D band to occupied states. Even the slight disorder in a sample of $x = 0.04$, exchanging less than 1.5% of Te, leads to strong and sheet-dependent decreases in electron scattering length. The signatures of fluctuating CDW gaps in both pure and substituted ZrTe_3 are observed, with a kink of the temperature dependence when long range order sets in in ZrTe_3 and less strong gapping and no kink in $\text{ZrTe}_{2.96}\text{Se}_{0.04}$.

Single-crystals of ZrTe_3 and $\text{ZrTe}_{2.96}\text{Se}_{0.04}$ have been grown by chemical vapour transport and characterised as described before [29]. For ARPES measurements, the samples were cleaved at the temperature $T = 7$ K and a vacuum of 10^{-10} mbar, exposing (001) surfaces as the samples cleave in the van-der-Waals gap between layers formed by $\text{Te}^{(2)}\text{-Te}^{(3)}$ atoms (inset in Fig. 1). ARPES data were acquired at beamline I05-ARPES [30] at T between 7 K and 290 K. The photon energy was set to $h\nu = 34$ eV and the energy resolution was chosen as $\delta E = 7$ meV with an angular resolution of less than 0.2° . The polarisation vector was kept in the (b, c) -plane of the crystal lattice (p -polarised). The k_x and k_y directions correspond to directions along the b -axis and approximately the a -axis, respectively.

Fig. 1 shows two FS maps for samples of pure ZrTe_3 and $\text{ZrTe}_{2.96}\text{Se}_{0.04}$. The labelling of high symmetry points acknowledges the effectively 2-dimensional electronic state observed in ARPES due to a surface relaxation [31]. This relaxation also leads to a splitting of observed bands, thus complicating the analysis. We selected $h\nu = 34$ eV, at which one component of the split bands dominates the spectra. At different $h\nu$ the same features are seen [31, 32], but strong contributions from both components would complicate the peak fitting analysis.

Analysing the differences between ARPES data from the two samples, first, we discuss the shape and position of bands near E_F . Second, we address the scattering rates as observed by peak widths. Finally, we discuss the temperature dependence of spectral weight at E_F . At first sight the features of the FS appear very similar, namely the almond shaped central

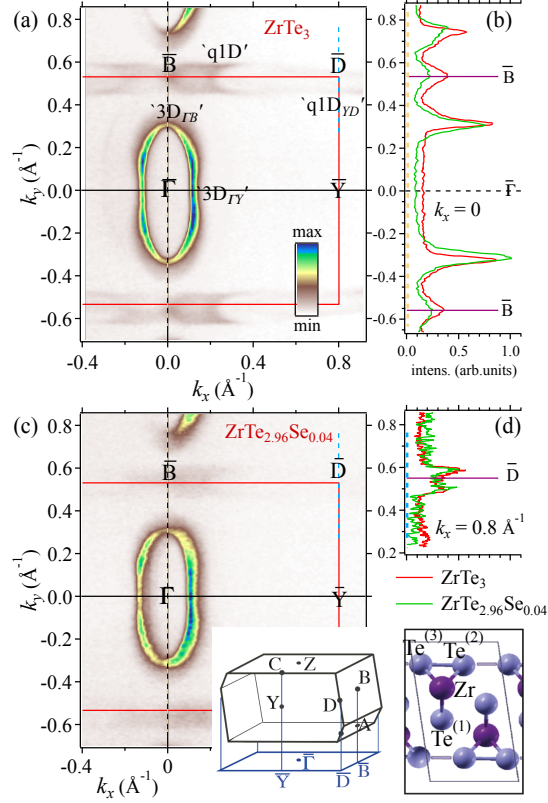


FIG. 1: FS maps of ZrTe_3 (a) and $\text{ZrTe}_{2.96}\text{Se}_{0.04}$ (c), acquired by ARPES at a temperature $T = 7$ K. The inset shows one unit cells of the crystal lattice of ZrTe_3 projected onto the (a, c) -planes and the Brillouin zone. The nearly equidistant Te chains adjacent to the van der Waals gap are highlighted by grey bars. Panels (b) and (d) show momentum distribution curves extracted from the maps along straight lines along k_y at two different k_x .

feature, labelled 3D [Fig. 1(a,c)]. In these maps, the pair of q1D sheets is of low intensity. Close to \bar{D} the intensity is further reduced by the suppression of spectral weight at the chemical potential (E_F) at low T [22, 31]. Close to \bar{B} at $k_x = 0.2 \text{ \AA}^{-1}$ two closing contours of this sheet are nevertheless clearly discernible.

Slicing into momentum distribution curves (MDCs) [Fig. 1(b, d) for $E = E_F$] reveals differences between the two data sets for the 3D FS sheet. The k_y wave vector along $\bar{\Gamma}$ - \bar{B} is reduced by 4% in $\text{ZrTe}_{2.96}\text{Se}_{0.04}$ when compared to ZrTe_3 . The k_x Fermi wave vector k_F along $\bar{\Gamma}$ - \bar{Y} is increased by 2%. Most remarkably, the k_F of the q1D bands close to \bar{D} are found to be identical within the error bars between both samples [Fig. 1(d)]. The k_F are

summarised in Tab. I. The anisotropy of the 3D sheet is thus slightly reduced and the FS volume is decreased in $\text{ZrTe}_{2.96}\text{Se}_{0.04}$ when compared to ZrTe_3 . From this reduction of FS volume we can estimate a reduction of hole-type carrier numbers in the 3D band of about 2%.

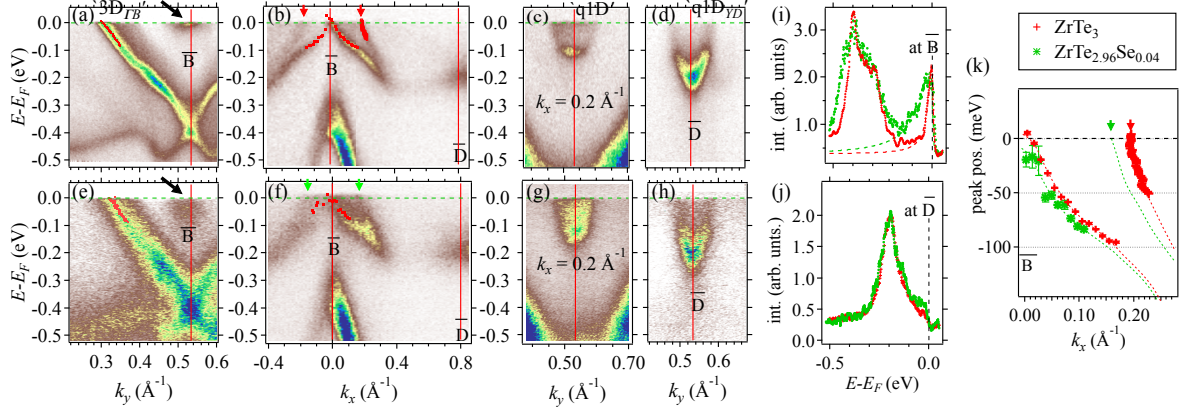


FIG. 2: ARPES dispersion cuts for ZrTe_3 (a, b, c, d) and $\text{ZrTe}_{2.96}\text{Se}_{0.04}$ (e, f, g, h) at $T = 7$ K. Red dots in panels (a, b, e, f) show the peak positions determined by numerical fits. A detailed view of these peak positions for the q1D bands along k_x close to \bar{B} is shown in panel (k). Energy distribution curves (EDCs) at high symmetry points are shown in (i) for \bar{B} and in (j) for \bar{D} for both samples. Dashed lines in panel (k) are drawn following the intensity traces in panels (b,f) as a guide to the eye.

From the easily observable k_F values along k_y ('q1D' at $k_x = 0.2 \text{ \AA}^{-1}$ and 'q1D_{YD}' at $k_x = 0.8 \text{ \AA}^{-1}$) the two q1D bands appear completely unchanged by the Se substitution. A close look is provided by the dispersion maps in Fig. 2(a-h). In Fig. 2(b) and (f) we trace the dispersion of the two bands along k_x by numerical fits. The summarised results in Fig. 2(k) reveal a decrease of the energy E of this band by -0.012 eV at \bar{B} . This results in a drastic change of the spectra at \bar{B} , marked by arrows in Fig. 2(a,e) and shown in Fig. 2(i). In pure ZrTe_3 this very sharp peak has been assigned to a vHS at E_F [22]. In $\text{ZrTe}_{2.96}\text{Se}_{0.04}$ the vHS is shifted to occupied states and the mechanism of sharpening the peak at low T [22] does not come into effect. In agreement with the shift of the lower q1D band k_F of the upper q1D band is also reduced from $k_x = 0.2 \text{ \AA}^{-1}$ in ZrTe_3 to $k_x = 0.13 \text{ \AA}^{-1}$ in $\text{ZrTe}_{2.96}\text{Se}_{0.04}$. The thus estimated shift of the upper q1D band (-50 meV at k_F) is larger than the shift of the lower q1D band (-12 meV).

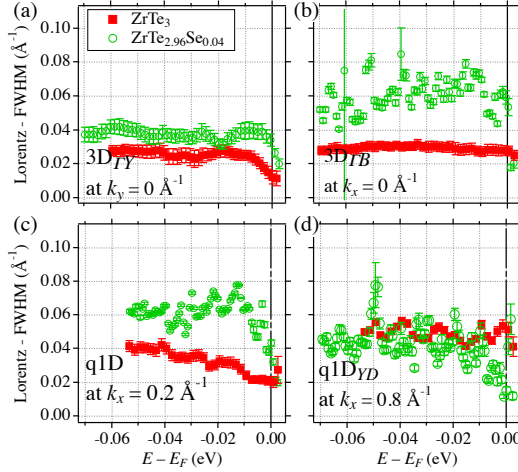


FIG. 3: Extracted peak widths at $T = 7$ K from fits to MDCs as a function of E for both samples. The corresponding peak positions are shown in Fig. 2. Panel (a) shows the 3D band along $\Gamma - Y$, at $k_y = 0$. Panel (b) shows the 3D band along $\Gamma - B$, at $k_x = 0$. Panel (c) shows the q1D band along k_y for $k_x = 0.2 \text{ \AA}^{-1}$ and (d) near \bar{D} .

At \bar{D} the peak position of the bottom of the q1D band is identical while the step height of intensity at E_F is larger in $\text{ZrTe}_{2.96}\text{Se}_{0.04}$ [Fig. 2(j)]. The T dependence of this intensity will be analysed below for further insight into CDW formation.

We now turn to the analysis of scattering rates. The results of MDC peak widths as a function of E are shown in Fig. 3. Standard numerical fitting was used to determine these widths with details given in Supplemental Material (SM) [32]. The widths are composed of two main contributions: a constant width due to impurity scattering plus an energy-dependent width due to EPC. The width due to EPC increases from zero at $E = E_F$ [33, 34] and saturates, in our data around $E - E_F = -0.01$ eV, which matches the range of phonons with strong EPC in ZrTe_3 [27, 28]. For example a pronounced width increase by 0.012 \AA^{-1} from 0.013 \AA^{-1} is observed at position ‘3D $_{\Gamma Y}$ ’ for ZrTe_3 [Fig. 3(a)]. Along k_y , at ‘3D $_{\Gamma B}$ ’ as well as ‘q1D’ (at $k_x = 0.2 \text{ \AA}^{-1}$) the data for $\text{ZrTe}_{2.96}\text{Se}_{0.04}$ show significantly higher widths throughout when compared to ZrTe_3 [Fig. 3(b,c)]. Near the \bar{D} point ‘q1D $_{YD}$ ’ we find basically identical data for both samples [Fig. 3(d)]. We note that error bars of the data from $\text{ZrTe}_{2.96}\text{Se}_{0.04}$ are generally larger than ZrTe_3 due to slightly different data acquisition settings. We consider the deviation of the two data sets at ‘q1D $_{YD}$ ’ very close to E_F as insignificant as the data points are compatible within these error bars. The thus extrapolated

TABLE I: Extracted values for k_F , the peak width δk , the Fermi velocity v_F and the thus estimated scattering rates for both samples. Four locations with dominant orbital character and contributing atoms are given.

location	character		$2k_F$ (\AA^{-1})	δk (\AA^{-1})	v_F (eV $\cdot\text{\AA}$)	$1/\tau$ (eV)		$2k_F$ (\AA^{-1})	δk (\AA^{-1})	v_F (eV $\cdot\text{\AA}$)
‘3D Γ_Y ’	Zr d	ZrTe ₃	0.633(3)	0.013(3)	4.0(2)	0.05(1)	ZrTe _{2.96} Se _{0.04}	0.622(5)	0.025(5)	4.5(2)
‘3D Γ_B ’	Te ⁽¹⁾ p_y , Zr d		0.232(2)	0.026(4)	1.8(2)	0.05(1)		0.244(3)	0.050(9)	2.1(2)
‘q1D’	Te ^(2,3) p_x		0.12(2)	0.02(1)	4.8(9)	0.10(5)		0.13(2)	0.04(1)	6.4(9)
‘q1D $_YD$ ’	Te ^(2,3) p_x		0.086(1)	0.05(2)	8.9(5)	0.44(20)		0.085(1)	0.03(2)	9.2(5)

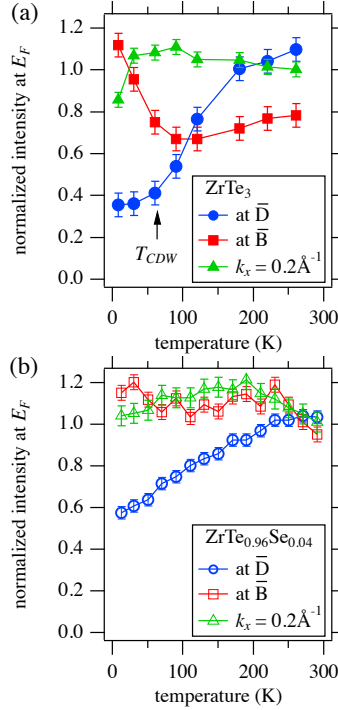


FIG. 4: Temperature dependence of the photoemission intensity at E_F from ZrTe₃ (a) and ZrTe_{2.96}Se_{0.04} (b). The intensities are summed up over a small range of $0.4 < k_y < 0.67 \text{ \AA}^{-1}$ at three different positions of k_x as indicated.

widths at E_F due to defect scattering are summarised in Tab. I. When multiplied with the Fermi velocity v_F they give an estimate of the scattering rate $1/\tau$ due to disorder. The scattering rate is enhanced upon Se substitution except for position ‘q1D $_YD$ ’ of the strongly nested CDW band [36].

Analysing the intensity at E_F as a function of T (Fig. 4) we find near constant values

for the 3D band (not shown) as well as for q1D near $k_x = 0.2 \text{ \AA}^{-1}$ (apart from a spurious lower intensity data point in $\text{ZrTe}_{2.96}\text{Se}_{0.04}$ at the lowest T). This is regular behaviour of the Fermi-Dirac distribution function without any modification of the bands or spectral weight. At $\bar{\text{B}}$, ZrTe_3 shows an upturn of intensity at low temperature, which is not observed in $\text{ZrTe}_{2.96}\text{Se}_{0.04}$ thus confirming the relation of this effect to the vHS [22][37]. Near $\bar{\text{D}}$ the drop of intensity sets in at room temperature (RT) in both samples and far above the structural transition T_{CDW} in ZrTe_3 . Thus both samples show the gap signature of fluctuating CDW [22]. In ZrTe_3 the gapping is strong with a 50% depletion of spectral weight at E_F at low T and the T -dependence shows a kink when long-range order sets in. In $\text{ZrTe}_{2.96}\text{Se}_{0.04}$ this T -dependence is near linear [Fig. 4(b)] and the depletion is less strong than in ZrTe_3 . The quenching of long-range order of the CDW is also confirmed by the absence of a PLD in x-ray diffraction from $\text{ZrTe}_{2.96}\text{Se}_{0.04}$ down to $T = 20 \text{ K}$ [32].

The orbital composition of the various bands has previously been analysed in detail in Ref. [20]. The dominant orbital character and contributing atoms are summarised in Tab. I and graphical representations are reproduced in SM [32]. Near $\bar{\text{D}}$ (points D or E of the bulk Brillouin zone), the q1D band is formed almost exclusively from Te p_x orbitals of the atoms $\text{Te}^{(2)}$ and $\text{Te}^{(3)}$ (orbitals oriented along the a -axis of the lattice). At $\bar{\text{B}}$ (bulk points B or A) and in the close vicinity of this point, significant contributions come from p_y orbitals of all three Te atoms, including $\text{Te}^{(1)}$. The 3D FS sheet is similarly composed of strong contributions from p_y of $\text{Te}^{(1)}$ as well as Zr d -orbitals. The observation of a large increase of scattering rates close to $\bar{\text{B}}$ and in the 3D FS sheet may thus arise from preferential incorporation of Se impurities in the $\text{Te}^{(1)}$ -site. Alternatively the pure one-dimensional character of the p_x -derived band near $\bar{\text{D}}$ may show suppressed defect scattering due to the phase space being reduced to only forward or full back-scattering [35].

In either case we note that the effects of the disorder is much more pronounced in the bands that show no gapping due to CDW formation, while the CDW-gapped portions of the FS are the locations of little change between ZrTe_3 and $\text{ZrTe}_{2.96}\text{Se}_{0.04}$. This region of the Brillouin zone was shown to couple strongly to phonons [28]. Our data show this EPC directly in several locations of momentum space by an increase of peak widths with decreasing E in the range of typical phonon energies. The EPC is similar in both samples and of similar magnitude as typical two-dimensional metals [33].

In conclusion, we find that the quenching of long-range CDW order with light isoelectronic

substitution in $\text{ZrTe}_{2.96}\text{Se}_{0.04}$ is driven by a decrease in the static scattering length. Our measurements thus confirm the structural disorder as the primary tuning parameter which dictates the phase diagram of $\text{ZrTe}_{3-x}\text{Se}_x$. The effects of disorder in the electronic spectral function are found to be sheet-dependent, detected as a significant increase in the linewidths of the 3D band and the q1D bands near $\bar{\text{B}}$, while no measurable additional broadening was found near $\bar{\text{D}}$. In addition, more subtle band shifts are observed, including a shift of the vHS at $\bar{\text{B}}$ away from the Fermi level to occupied states. These band shifts are not considered as driving forces of the CDW quenching. A continuous partial loss of DOS around $\bar{\text{D}}$ as a function of T is interpreted as a signature of a fluctuating CDW as in previous work [22]. This is expected to weaken the SC and the shift of the vHS will also reduce the DOS at E_F when compared to ZrTe_3 . The reduction of DOS from the region around $\bar{\text{D}}$ is less strong in $\text{ZrTe}_{2.96}\text{Se}_{0.04}$ than in ZrTe_3 and lacks the kink signature of long-range order that is observed in ZrTe_3 . Thus SC can emerge despite CDW fluctuations.

We are grateful to F. Baumberger for use of his ARPES data analysis software and to Diamond Light Source, where access to beamline I05 (NT11039, SI13797, and NT17065) and beamline I19 (MT8776) contributed to the results presented here. We acknowledge technical assistance for the ARPES experiments by Z. K. Liu and L. C. Rhodes and help with x-ray diffraction experiments was provided by S. Barnes, H. Novell, F. Fabrizi and D. Allen. Work at Brookhaven National Laboratory was supported by the U.S. Department of Energy, Office of Science, Office of Basic Energy Sciences, under Contract No. DE-SC0012704.

* Present and permanent address: High Magnetic Field Laboratory, Chinese Academy of Sciences - Hefei 230031, PRC

- [1] G. Grüner, *Density Waves in Solids*, vol. 89 of *Frontiers in Physics* (Perseus publishing, Cambridge MA, 1994).
- [2] P. Monceau, *Advances in Physics* **61**, 325 (2012).
- [3] G. Ghiringhelli, M. Le Tacon, M. Minola, S. Blanco-Canosa, C. Mazzoli, N. B. Brookes, G. M. De Luca, A. Frano, D. G. Hawthorn, F. He, et al., *Science* **337**, 821 (2012).
- [4] J. Chang, E. Blackburn, A. T. Holmes, N. B. Christensen, J. Larsen, J. Mesot, R. Liang, D. A. Bonn, W. N. Hardy, A. Watenphul, et al., *Nat Phys* **8**, 871 (2012).

- [5] M. Le Tacon, A. Bosak, S. M. Souliou, G. Dellea, T. Loew, R. Heid, K.-P. Bohnen, G. Ghiringhelli, M. Krisch, and B. Keimer, *Nat Phys* **10**, 52 (2014).
- [6] P. Anderson, *Journal of Physics and Chemistry of Solids* **11**, 26 (1959).
- [7] S. Tang, V. Dobrosavljević, , and E. Miranda, *Phys. Rev. B* **93**, 195109 (2016).
- [8] A. Petrovic, D. Ansermet, D. Chernyshov, M. Hoesch, D. Salloum, P. Gougeon, M. Potel, L. Boeri, and C. Panagopoulos, *Nature Communications* **7** (2016).
- [9] M. Nunez-Regueiro, J.-M. Mignot, M. Jaime, D. Castello, and P. Monceau, *Synthetic Metals* **56**, 2653 (1993).
- [10] R. Yomo, K. Yamaya, M. Abliz, M. Hedo, and Y. Uwatoko, *Phys. Rev. B* **71**, 132508 (2005).
- [11] A. Sacchetti, C. L. Condon, S. N. Gvasaliya, F. Pfner, M. Lavagnini, M. Baldini, M. F. Toney, M. Merlini, M. Hanfland, J. Mesot, et al., *Phys. Rev. B* **79**, 201101 (2009).
- [12] J. J. Hamlin, D. A. Zocco, T. A. Sayles, M. B. Maple, J. H. Chu, and I. R. Fisher, *Phys. Rev. Lett.* **102**, 177002 (2009).
- [13] D. A. Zocco, J. J. Hamlin, K. Grube, J.-H. Chu, H.-H. Kuo, I. R. Fisher, and M. B. Maple, *Phys. Rev. B* **91**, 205114 (2015).
- [14] L. J. Li, T. O. O'Farrell, K. P. Loh, G. Eda, B. Özyilmaz, and A. H. C. Neto, *nature* **529**, 185 (2016).
- [15] E. Revolinsky, G. A. Spiering, and D. J. Beerntsen, *Journal of Physics and Chemistry of Solids* **26** (6), 1029 (1965).
- [16] J. A. Wilson, F. J. D. Salvo, and S. Mahajan, *Advances in Physics* **24** (2), 117 (1975).
- [17] S. Takahashi, S. Sambongi, and S. Okada, *J. Phys. (Paris) Colloq.* **44**, C3 (1983).
- [18] S. Tsuchiya, K. Matsubayashi, K. Yamaya, S. Takayanagi, S. Tanda, and Y. Uwatoko, *New Journal of Physics* **19**, 063004 (2017).
- [19] J. A. Wilson, *Phys. Rev. B* **19**, 6456 (1979).
- [20] C. Felser, E. Finckh, H. Kleinke, and W. Tremel, *J. Mater. Chem.* **8**, 1787 (1998).
- [21] K. Stöwe and F. Wagner, *J. Solid State Chem.* **138**, 160 (1998).
- [22] T. Yokoya, T. Kiss, A. Chainani, S. Shin, and K. Yamaya, *Phys. Rev. B* **71**, 140504(R) (2005).
- [23] X. Zhu, B. Lv, F. Wei, Y. Xue, B. Lorenz, L. Deng, Y. Sun, and C.-W. Chu, *Phys. Rev. B* **87**, 024508 (2013).
- [24] S. L. Gleason, Y. Gim, T. Byrum, A. Kogar, P. Abbamonte, E. Fradkin, G. J. MacDougall, D. J. Van Harlingen, X. Zhu, C. Petrovic, et al., *Phys. Rev. B* **91**, 155124 (2015).

- [25] C. W. Kwang-Hua, Chemical Physics **409**, 37 (2012).
- [26] M. Hoesch, G. Garbarino, C. Battaglia, P. Aebi, and H. Berger, Phys. Rev. B **93**, 125102 (2016).
- [27] M. Hoesch, A. Bosak, D. Chernyshov, H. Berger, and M. Krisch, Phys. Rev. Lett. **102**, 086402 (2009).
- [28] Y. Hu, F. Zheng, X. Ren, J. Feng, and Y. Li, Phys. Rev. B **91**, 144502 (2015).
- [29] X. Zhu, W. Ning, L. Li, L. Ling, R. Zhang, J. Zhang, K. Wang, Y. Liu, L. Pi, Y. Ma, et al., Scientific Reports **6**, 26974 (2016).
- [30] M. Hoesch, T. K. Kim, P. Dudin, H. Wang, S. Scott, P. Harris, S. Patel, M. Matthews, D. Hawkins, S. G. Alcock, et al., Review of Scientific Instruments **88**, 013106 (2017).
- [31] M. Hoesch, X. Cui, K. Shimada, C. Battaglia, S.-i. Fujimori, and H. Berger, Phys. Rev. B **80**, 075423 (2009).
- [32] *Supplemental material* (2018), URL to be inserted by editor.
- [33] F. Reinert, B. Eltner, G. Nicolay, F. Forster, S. Schmidt, and S. H ufner, Physica B: Condensed Matter **351**, 229 (2004).
- [34] J. Jiang, K. Shimada, H. Hayashi, H. Iwasawa, Y. Aiura, H. Namatame, and M. Taniguchi, Phys. Rev. B **84**, 155124 (2011).
- [35] T. Giamarchi, *Quantum Physics in One Dimension*, vol. 121 of *International Series of Monographs on Physics* (Oxford Science Publications, 2003).
- [36] As the CDW formation could lead to an additional band dispersion due to back-folding, one could expect a T -dependent additional broadening. No such broadening is, however, observed and the evolution across T_{CDW} is smooth in the SM Figures S2 and S3 [32].
- [37] As the vHS affects only a small portion of the FS the significance for the DOS at E_F is small